Taylor & Francis
Taylor & Francis Group

Numerical Heat Transfer, Part A: Applications
An International Journal of Computation and Methodology

ISSN: 1040-7782 (Print) 1521-0634 (Online) Journal homepage: https://www.tandfonline.com/loi/unht20

A numerical study on determination of volume averaged thermal transport properties of metal foam structures using X-ray microtomography technique

Hasan Celik, Moghtada Mobedi, Akira Nakayama & Unver Ozkol

To cite this article: Hasan Celik, Moghtada Mobedi, Akira Nakayama & Unver Ozkol (2018) A numerical study on determination of volume averaged thermal transport properties of metal foam structures using X-ray microtomography technique, Numerical Heat Transfer, Part A: Applications, 74:7, 1368-1386, DOI: 10.1080/10407782.2018.1494936

To link to this article: https://doi.org/10.1080/10407782.2018.1494936

NUMERICAL HEAT TRANSFER, PART A
2018, VOL. 74, NO. 7, 1368–1386
https://doi.org/10.1080/10407782.2018.1494936

A numerical study on determination of volume averaged thermal transport properties of metal foam structures using X-ray microtomography technique

Hasan Celik[a,b], Moghtada Mobedi[b], Akira Nakayama[b,c], and Unver Ozkol[a]

[a]Mechanical Engineering Department, Izmir Institute of Technology, Urla, Izmir, Turkey; [b]Faculty of Engineering, Shizuoka University, Naka-ku, Hamamatsu, Japan; [c]School of Civil Engineering and Architecture, Wuhan Polytechnic University, Wuhan, Hubei, China

ABSTRACT

Volume averaged thermal transport properties of two metal foams with 10 and 20 PPI are obtained by using microtomography technique. The digital 3D structures of samples are generated in computer environment. The governing equations are solved for the entire domain and the volume averaged technique is used to determine interfacial heat transfer coefficient, longitudinal and transverse thermal dispersion conductivity. The study is performed for the pore scale Reynolds number from 100 to 600. The obtained results are within the ranges of the suggested correlations in literature. The present study supports the correlations suggested by Calmidi and Mahajan (2000) and Zhang et al. (2016).

ARTICLE HISTORY
Received 1 April 2018
Accepted 26 June 2018

1. Introduction

Metal foams are consolidated porous structures with high porosity and low density. The effects of both the large number of ligaments mixing fluid and sizable interfacial surface area between solid and fluid phases improve heat transfer rate significantly. These advantages of metal foams attracted the attention of researchers studying on the enhancement of heat transfer. The main disadvantage of metal foams is high pressure drop comparing to other passive heat transfer enhancement methods which increases pumping power. Despite this disadvantage, metal foams are used in different heat transfer areas from cooling of electronic equipment to cooling of rocket jackets.

Two main approaches are widely employed for simulations of heat and fluid flow in porous media such as metal foams. Each approach has its advantages and drawbacks. Pore scale method (PSM) is one of two approaches; in which the governing equations for solid or fluid are solved directly, and therefore, the velocity, temperature and pressure fields are obtained precisely. Despite yielding accurate results, the application of PSM is very cumbersome and impractical due to considerable number of pores in a porous medium. Volume-averaged method (VAM) has been discovered to overcome this difficulty. In VAM, the governing equations are integrated over a representative volume of porous media and volume-averaged governing equations (i.e., macroscopic governing equations) are derived. Therefore, the discontinuity of phases is removed and the achieved governing equations can be solved for the entire continuous domain. The major drawback of VAM is the appearance of new terms in the governing equations due to the space

CONTACT Moghtada Mobedi moghtada.mobedi@shizuoka.ac.jp Faculty of Engineering, Shizuoka University, 3-5-1 Johoku, Naka-ku, Hamamatsu 432-8561, Japan
Color versions of one or more of the figures in the article can be found online at www.tandfonline.com/unht.

Nomenclature

$< >$	volume average indicator
A	area
C	inertia coefficient
C_p	specific heat capacity at constant pressure [J/kg K]
hv	volumetric interfacial convective heat transfer coefficient [W/m^3 K]
k	thermal conductivity [W/m K]
K	permeability [m^2]
Nu	Nusselt number
p	pressure [Pa]
Re	Reynolds number
T	temperature [K]
u	velocity vector [m/s]
V	volume [m^3]

Greek symbols

ε	porosity
μ	dynamic viscosity [Pa s]
ν	kinematic viscosity [m^2/s]
ρ	density [kg/m^3]

Subscript and superscript

$'$	deviation
*	effective
c	cell
dis	dispersion
f	fluid
int	interface
ref	reference
s	solid
stag	stagnant
tor	tortuosity
v	volumetric

integration. Those terms involve parameters, known as volume averaged transport properties (i.e., macroscopic transport parameters). The precise value of transport properties is the crucial point for obtaining accurate results by employing VAM. Volume averaged transport properties can be obtained experimentally and/or theoretically. Recent developments in computing technology and microimage techniques allow researchers to obtain accurate volume averaged transport properties, numerically.

For volume averaged governing equations for heat and fluid flow in metal foams (when the radiation effect is neglected, the flow is incompressible, and the fluid is Newtonian) generally five macroscopic transport properties as permeability, inertia coefficient, stagnant thermal conductivity (involving tortuosity effect), interfacial heat transfer coefficient, and thermal dispersion conductivity should be known [1, 2]. The number of experimental and numerical studies on determination of permeability and inertia coefficient of different kinds of metal foams is high [3–5]. However, the number of studies on the volume averaged transport properties for energy equation which are interfacial heat transfer coefficient, longitudinal and transverse thermal dispersion conductivities is too limited and further studies on these transport properties for the metal foam are needed. A brief literature survey on the studies on these parameters is presented below.

Interfacial heat transfer coefficient: Local thermal equilibrium (LTE) may not be an appropriate assumption when the volume-averaged temperature difference between fluid and solid phases is considerably different than macro-scale temperature difference. LTE may fail during the early stages of heat transfer or may fail when the interaction between the fluid and solid phases is not sufficient due to different reasons such as small heat transfer area. The heat transfer at interface of two phases can be modeled by defining an interfacial convective heat transfer coefficient. Literature survey shows that most of the numerical studies on determination of interfacial convective heat transfer coefficient were done for porous media with periodic structures such as the numerical studies of Kuwahara et al. [6] Saito and de Lamos [7], Ozgumus and Mobedi [8]. Recent developments in microtomography technique allow researchers to model a stochastic porous structure in computer environment by taking images in microscale resolution and then generate the digital structure of the foam by using an appropriate image processing software. The number of reported studies on the determination of the interfacial convective heat transfer coefficient of metal foams by the microtomography technique is limited. Vijay et al. [9] obtained

porosity, pore diameter, strut diameter, and specific surface area by the microtomography method and then experimentally obtained the interfacial convective heat transfer coefficient based on the correlation of Zukauskas [10] for ceramic foams. Zafari et al. [11] studied the determination of interfacial convective heat transfer coefficient of aluminum and copper metal foams with porosity from 0.85 to 0.95 by employing the microtomography technique. A correlation for determination of the interfacial heat transfer coefficient as a function of Re number based on permeability was suggested. Kamiuto and Yee [12] employed experimental data obtained by several researchers to suggest a general correlation for volumetric interfacial heat transfer coefficient of open-cellular porous media. They suggested an equivalent strut diameter as characteristic length. An experimental study on the interfacial heat transfer coefficient of aluminum foam was performed by Calmidi and Mahajan [13]. The suggested correlation based on Zukauskas correlation [10]. The strut diameter is used as characteristic length. The list of the suggested correlations and their comparison are presented and discussed in the later section.

Thermal dispersion conductivity: Thermal dispersion occurs due to different reasons such as non-uniformity of temperature and velocity fields, fluctuations of flow, splitting and/or rejoining of flow along the flow path. It can enhance heat transfer drastically. Thermal dispersion conductivity can be calculated experimentally or theoretically. Similar to the interfacial convective heat transfer coefficient, computational determination of thermal dispersion mostly is reported for periodic structures such as the studies of Kuwahara and Nakayama [14], Ozgumus and Mobedi [15]. Two experimental studies as the study of Calmidi and Mahajan [13] and Vijay et al. [9] on the determination of transverse thermal dispersion for metal foam and alumina ceramic foam have been reported in the literature. Calmidi and Mahajan [13] suggested a correlation in terms of permeability based Re number while the correlation suggested by Vijay et al. [9] is based on channel Re number. Furthermore, Zhang et al. [16] used conduit model and suggested a correlation both for longitudinal and transverse thermal dispersion for metal foams. They derived their correlations for thermal dispersion by using the correlation of Calmidi and Mahajan [13] suggested for the interfacial heat transfer coefficient. Their suggested correlation for the longitudinal thermal dispersion might be the only available correlations in literature for metal foams. The list of the suggested correlations for thermal dispersion conductivity will be presented later in Section 4.

The aim of this study is the determination of interfacial heat transfer coefficient and thermal dispersion for both longitudinal and transverse directions by using microtomography techniques. Aluminum foams with the pore density of 10 and 20 PPI are studied. These foam structures were scanned using a microtomography device, and then 3D digital structures are generated in the computer environment. After that, the mesh is generated, and a solver package is used to solve the continuity, momentum and energy equations in pore scale. By applying volume averaged technique to the temperature and velocity fields, the interfacial heat transfer coefficient and thermal dispersion conductivity are calculated. Our literature survey showed that the number of computational studies on determination of volume averaged thermal transport properties of metal foams particularly on thermal dispersion conductivity is too limited. This study presents significant information on utilization of microtomography technique for analyzing heat transfer in porous media and determination of thermal dispersion conductivity by using this technique.

2. A background on pore scale and volume averaged heat and fluid flow equations

As it was mentioned before, there are two main approaches for analyzing heat and fluid flow in porous media. The first one is PSM in which the governing equations are written for solid and fluid in pore scale. They can be simplified and solved for the considered domain (such as fully developed assumption), or they can be solved in primitive form. For the present problem since the fluid is Newtonian and the flow is incompressible and steady state, the following governing equations are valid for solid and fluid phases:

$$\nabla \cdot \vec{u} = 0 \tag{1}$$

$$\rho_f \vec{u} \cdot \nabla \vec{u} = -\nabla p + \mu \nabla^2 \vec{u} \tag{2}$$

$$(\rho C_p)_f \vec{u} \cdot \nabla T_f = k_f \nabla^2 T_f \tag{3}$$

$$k_s \nabla^2 T_s = 0 \tag{4}$$

where $\vec{u}$ is the velocity vector, p is the pressure, ρ is the density of the air, and μ is the kinematic viscosity.

The second popular approach for analyzing heat and fluid flow in porous media is the VAM. A scalar or vector quantity can be integrated over a control volume in a porous medium. Since two phases as solid and fluid exist in a porous medium, two volume averaged quantity can be defined:

$$\langle \varphi \rangle = \frac{1}{V} \int_V \varphi \mathrm{d}V \tag{5}$$

$$\langle \varphi \rangle^x = \frac{1}{V_x} \int_{V_x} \varphi \mathrm{d}V \tag{6}$$

which are called as volume averaged and intrinsic volume averaged of φ quantity, respectively. V and $V_x$are the total volume and corresponding volume of phase of x phase which might be solid or fluid. If Eqs. (1)–(4) are integrated over a control volume of a porous medium, the following volume average transport equations can be found by using some assumptions and mathematical manipulations [17, 18]:

$$\nabla \cdot \langle \vec{u} \rangle = 0 \tag{7}$$

$$\frac{1}{\varepsilon^2} \langle \vec{u} \rangle \cdot \nabla \langle \vec{u} \rangle = -\frac{1}{\rho_f} \nabla \langle p \rangle^f + \frac{\mu}{\varepsilon} \nabla^2 \langle \vec{u} \rangle - \frac{\mu}{\rho_f K} \langle \vec{u} \rangle - \frac{C}{K^{1/2}} |\langle \vec{u} \rangle| \langle \vec{u} \rangle \tag{8}$$

$$\varepsilon (\rho C_p)_f \langle \vec{u} \rangle \cdot \nabla) \langle T \rangle^f = \varepsilon \nabla . (k_f \nabla \langle T \rangle^f) + \frac{1}{V} \nabla \left(\int_{A_{int}} k_f T^f \mathrm{d}A \right) - (\rho C_p)_f \varepsilon \nabla \langle T' u' \rangle^f - \frac{1}{V} \int_{A_{int}} k_f \nabla T^f \cdot \vec{n} \, \mathrm{d}A \tag{9}$$

$$\nabla \cdot k_s (1-\varepsilon) \nabla \langle T \rangle^s = \frac{1}{V} \nabla \left(\int_{A_{int}} k_s T^s \mathrm{d}A \right) + \frac{1}{V} \int_{A_{int}} k_s \nabla T^s \cdot \vec{n} \mathrm{d}A \tag{10}$$

As can be seen, the continuity equation is not changed. However, some new terms appeared in the momentum equation due to volume average process. The last two terms in the momentum equation represent viscous and inertia effects of flow in the porous media due to large solid surface area. There are three new terms in the fluid phases energy equation (last three terms) represent the effects of thermal tortuosity, thermal dispersion and heat transfer between solid and fluid phases. In the energy equation for solid phase, two new terms relating to tortuosity and heat transfer between solid and fluid phases exist. There is no doubt that, the above new terms should be written in an appropriate form to make the solution of those equations possible. The definition of interfacial heat transfer coefficient is used to provide an appropriate form for last terms of Eqs. (9) and (10). The interfacial heat transfer coefficient is defined based on the volume averaged heat transfer rate between solid and fluid, and the difference between the volume average temperature of solid and fluid.

$$\frac{1}{V} \int_{A_{int}} k_f \nabla T_f \cdot \vec{n} \mathrm{d}V = h_{int} \left(\langle T \rangle^s - \langle T \rangle^f \right) \tag{11}$$

The effect of tortuosity can be written in terms of gradient of macroscopic temperature as follows:

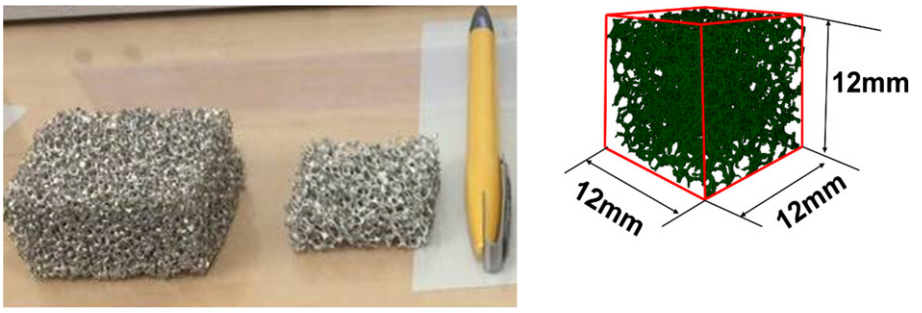

Figure 1. The considered 10 PPI and 20 PPI pore density metal foams (*a*) the real structure, (*b*) the studied domain generated in computer environment (20 PPI).

$$k_{tor,f}\nabla\langle T\rangle^f = \frac{1}{V}\int_{A_{int}} k_f T^f \mathrm{d}A \tag{12}$$

$$k_{tor,s}\nabla\langle T\rangle^s = \frac{1}{V}\int_{A_{int}} k_s T^s \mathrm{d}A \tag{13}$$

$k_{tor,f}$ and $k_{tor,s}$ can be called as tortuosity thermal conductivity for solid and fluid phases. Since both the stagnant thermal and tortuosity conductivities do not involve velocity quantity, some of researchers prefer to combine the stagnant thermal conductivity and tortuosity effect as follows:

$$k_{stag,s} = (1-\varepsilon)k_s + k_{tor,s} \tag{14}$$

$$k_{stag,f} = \varepsilon k_f + k_{tor,f} \tag{15}$$

$k_{stag,s}$ and $k_{stag,f}$ are the effective stagnant thermal conductivity for solid and fluid phases. Yang et al. [19] stated that for the heat and fluid flow in porous media with high thermal conductivity ratio between solid and fluid phases (such as aluminum-air) the effective thermal conductivity for diffusion term could be defined as:

$$\varepsilon^* = \frac{2+\varepsilon}{3} \tag{16}$$

and then the stagnant thermal conductivity can be found as:

$$k_{stag,s} = (1-\varepsilon^*)k_s = \frac{1-\varepsilon}{3}k_s \tag{17}$$

$$k_{stag,f} = \varepsilon^* k_f = \frac{2+\varepsilon}{3}k_f \tag{18}$$

Finally, the term relating to thermal dispersion in Eq. (10) can also be written in terms of volume averaged (macroscopic) temperature gradient, hence;

$$k_{disp}\nabla\langle T\rangle^f = \nabla\cdot(\rho C_p)_f\langle T'u'\rangle \tag{19}$$

Based on the above definitions, Eqs. (9) and (10) take the following form:

$$\varepsilon\rho_f c_{p_f}\langle\vec{u}\rangle\cdot\nabla\langle T\rangle^f = \nabla\cdot\left(k_{stag,f}+\varepsilon k_{disp}\right)\nabla\langle T\rangle^f + h_v\left(\langle T\rangle^s - \langle T\rangle^f\right) \tag{20}$$

$$\nabla\cdot\left(k_{stag,s}\right)\nabla\langle T\rangle^f - h_v\left(\langle T\rangle^s - \langle T\rangle^f\right) = 0 \tag{21}$$

Hence, in order to find the volume averaged temperature, five coefficients which are permeability and inertia coefficients (to find velocity field), stagnant and dispersion thermal conductivity, and interfacial heat transfer coefficient should be known. The present paper studies the numerical

Table 1. Some properties obtained from 3D model generated in computer environment.

Sample no.	1	2
Pore density (PPI)	10	20
Material	Al T-6201	Al T-6201
Porosity	0.90	0.95
Cell diameter [m]	0.0044	0.0023
Strut diameter [m]	0.00028	0.00019
Surface area [$m^{2/}$ m^3]	868	1,603
Average permeability [m^2] [20]	1.83E − 07	9.92E − 08

determination of the last two coefficients which are interfacial heat transfer coefficient and dispersion thermal conductivity for two metal foams by using the microtomography technique.

3. Considered metal foam, image processing and computational details

The studied metal foam structures are given in Figure 1*a*. Air is taken as working fluid, and the effect of gravity is neglected. Table 1 shows the structural parameters of studied metal foams as pore diameter, cell diameter, strut thickness, and specific surface area. Thermophysical properties of air and aluminum are taken as constant.

The method for determination of transport volume-averaged parameters by using microtomography can be divided into four steps as:

- Microscanning of the structures and obtaining of images.
- Processing of the images and obtaining an appropriate digital 3D structure computational main in computer environment.
- Generating mesh for the structured domain and solving pore scale governing equations.
- Determination of macroscopic transport properties by taking volume average of the obtained velocity and temperature field.

The details of these steps for the present problem are explained in the following subsections.

3.1. Microscanning the structures and obtaining the images

X-ray computed microtomography is one of the widely used nondestructive methods for analyzing the structure of materials. In a microtomography scanner, X-ray beam cone passes through the sample and it is collected by a detector. The sample is rotated providing a series of 2D projection images at different angles. After completing scanning process, the digital structure of sample may be obtained in computer environment from 2D images. In this study, the aluminum foam samples with pore density of 10 PPI with dimensions of $40 \times 40 \times 35\,mm^3$ and 20 PPI with dimensions of $40 \times 40 \times 20\,mm^3$ were received from a manufacturer as shown in Figure 1*a*. Since, the determination of velocity and temperature for the entire samples is almost impossible for the authors, due to the limitations of computational resources, the microtomography images are obtained only for representative elementary volume (REV) with the size of $12 \times 12 \times 12\,mm^3$ as shown in Figure 1*b*. The studied REV is scanned by $9 \times 9\,\mu m^2$ as pixel size and $13.6\,\mu m$ as voxel length, approximately. This means that the number of pixels in both x and y directions are around 1,400 and the number of acquired images is 927.

3.2. Processing of the images and obtaining an appropriate digital 3D structure

Following the scanning procedure, the obtained images are processed in ImageJ software. The obtained images from X-ray microtomography are processed into black and white regions. Otsu

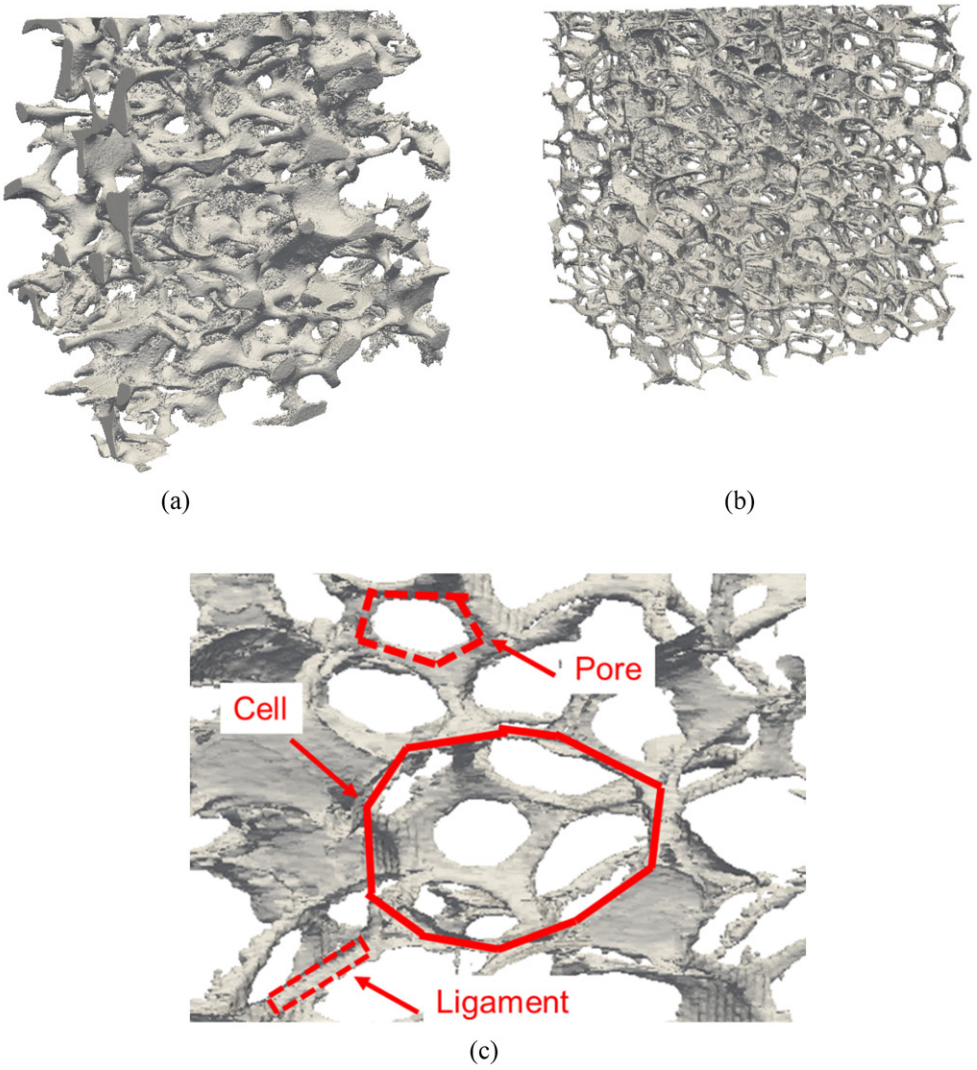

Figure 2. The foam samples generated in computer environment; (*a*) 10 PPI aluminum foam, (*b*) 20 PPI aluminum foam, (*c*) cell dimension, pore and ligament in the structured metal foam with 20 PPI.

method is used as a threshold method to reduce a gray level image to a binary image. Processing images in the computer environment is expensive procedure since high amount of random access memory (RAM) is required. Around 32GB RAM is used to process the images and 3D domain is obtained as STereoLithography (STL) file. Figure 2*a*, *b* shows the obtained digital structures of the studied metal foams for 10 and 20 PPI. Figure 2*c* shows a close view of cells for aluminum foam with 20 PPI. The cells, pores, and ligaments can be recognized clearly and their sizes are measured in computer environment.

3.3. Generating mesh and solving pore scale governing equations

After obtaining STL file, snappyHexMesh mesh generator package is used to generate hexahedral mesh for the obtained 3D domain in the computer environment. The generated meshes for aluminum foam with 10 and 20 PPI are shown in Figure 3. Following mesh generation, CFD model can be constructed. Since a pore level simulation is done, Eqs. (1)–(4) are solved, iteratively.

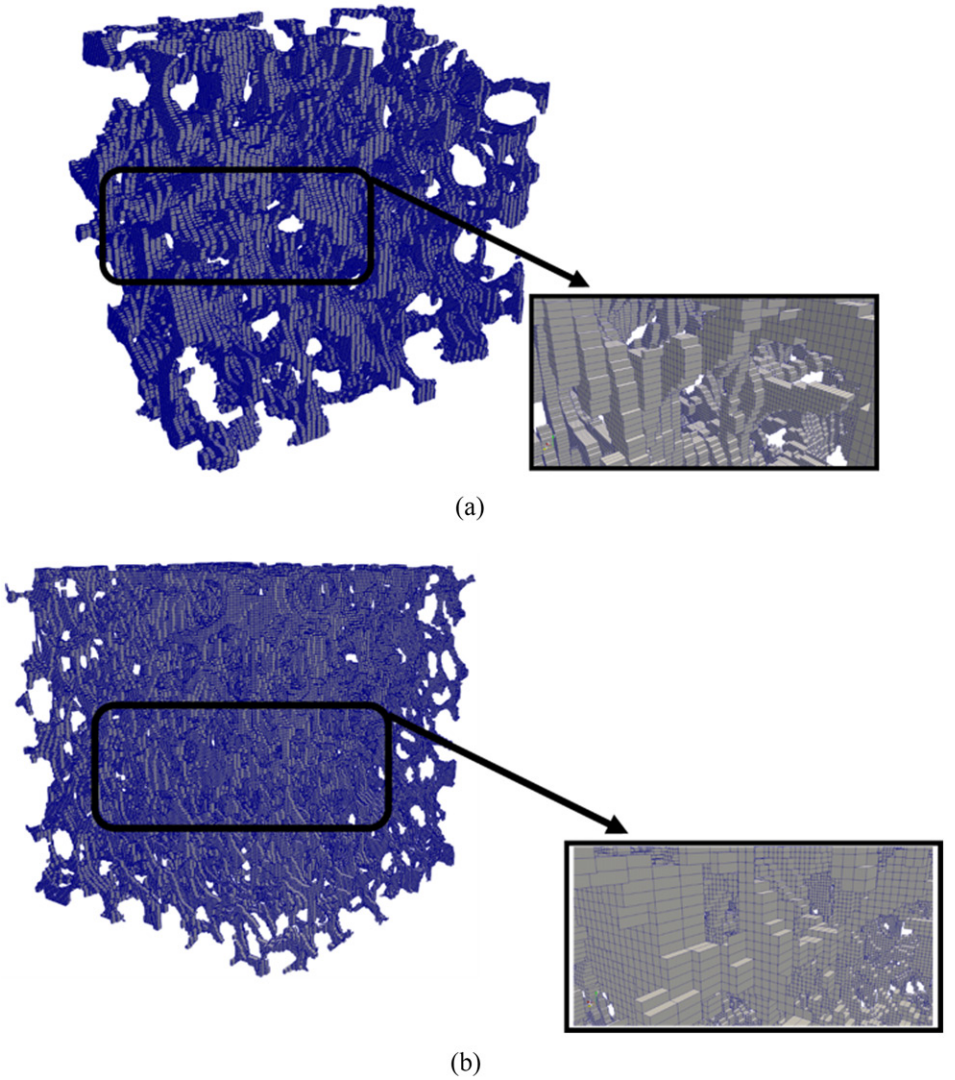

Figure 3. The generated domain and voxels in computer environment; (*a*) 10 PPI metal foam, (*b*) 20 PPI metal foam.

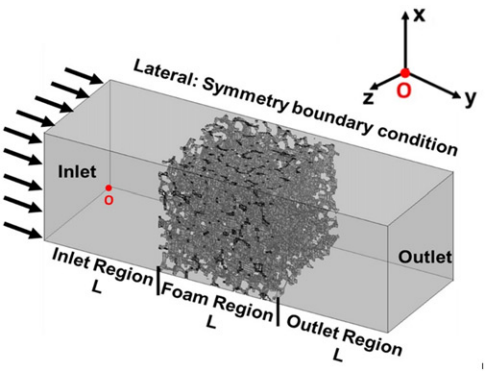

Figure 4. The considered domain with dummy inlet and outlet regions, and boundary conditions (O indicates the origin point).

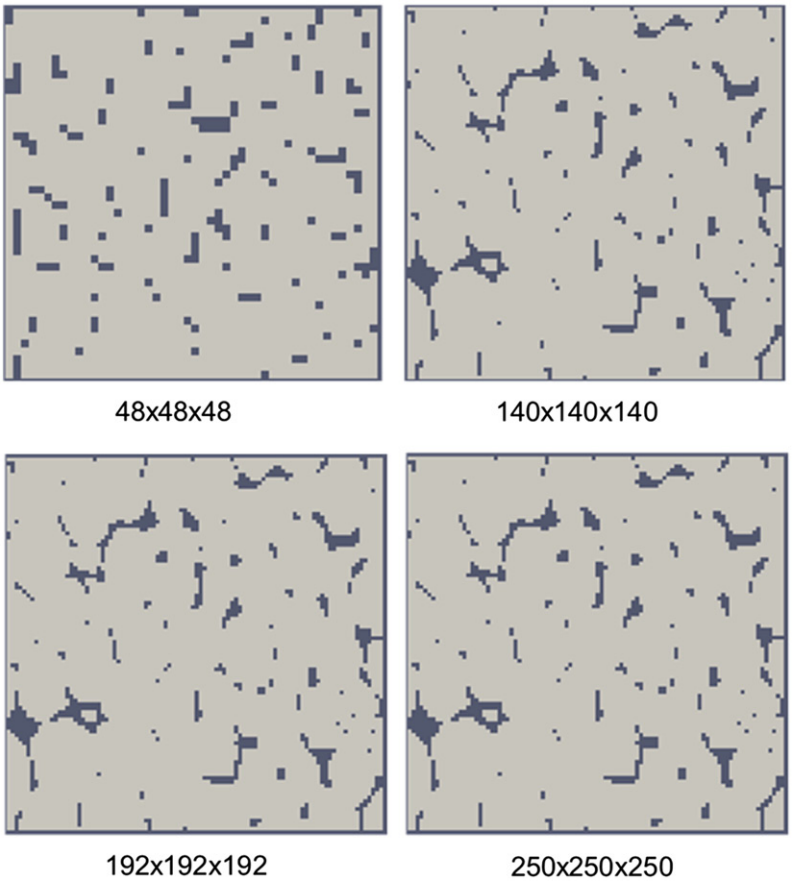

Figure 5. The change of the generated structure of aluminum foam with PPI =20 with number of grids for the surface with $y = 3L/2$ (black is solid region while gray represents void).

For reducing the inlet and outlet effects, dummy regions are added to the computational domain before and after the foam section as shown in Figure 4. The dimensions of these dummy regions are the same with the dimensions of the foam region. OpenFOAM 2.3.x based on finite volume method is used in this study. All terms in the governing equations are discretized by second order central differencing schemes. The velocity and pressure coupling is discretized by SIMPLE algorithm. The convergence criterion, which is the maximum value of the difference between each iteration step, is set to 10^{-6} for all the terms in the governing equations.

A uniform velocity is applied to the inlet section, and the boundary condition of zero gradient for velocity and temperature is applied for the outlet referring to the negligible diffusion transport. A slip boundary condition is applied to the lateral walls of the channel in order to reduce the effect of wall on the heat and flow fields. The computational domain and boundary conditions are also shown in Figure 4.

It should be mentioned that $k_s \gg k_f$ $(k_s/k_f \approx 6,000)$ and ligament diameter is small (0.19 mm), the control volume is thin (12 mm) and working fluid is air. This situation permits researchers to apply constant temperature assumptions for solid phase. Hence, there might be no need to solve the heat conduction equation for solid (Eq. (10)). The same assumption has been used by many researchers such as Saito and de Lamos [7] and Ozgumus and Mobedi [8].

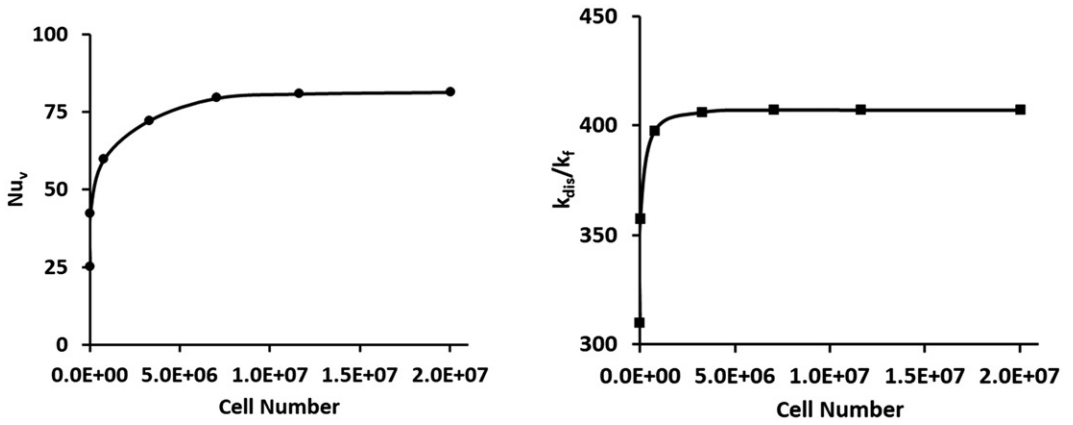

Figure 6. Validation of number of grids for Re =600; (*a*) the change of volumetric Nusselt number in *y* direction with respect to cell number, (*b*) the change of longitudinal thermal dispersion ratio in *y* direction respect to cell number.

3.4. Application of volume average technique to determine macroscopic transport properties

After obtaining temperature, pressure, and velocity distributions in the solid and fluid phases, the value of interfacial heat transfer coefficient and thermal dispersion conductivity can be calculated by using volume average technique. Fortunately, most of the commercial software permits the numerical integration of a quantity in a domain. Before presenting the related equations for determination of macroscopic thermal properties, it should be mentioned that the interfacial heat transfer coefficient is a scalar quantity independent from the direction. However, thermal dispersion is a tensor quantity whose value depends on the direction. This study focuses on the value of the longitudinal (X direction) and transverse (Y) of thermal dispersion conductivity when fluid flows longitudinally. Eqs. (22)–(24) can be used to determine the interfacial heat transfer coefficient, and longitudinal and transverse thermal dispersion coefficients.

$$h_{int} = \frac{\frac{1}{V}\int_{A_{int}} k_f \nabla T_f \cdot \vec{n}\,\mathrm{d}V}{\left(\langle T\rangle^s - \langle T\rangle^f\right)} \tag{22}$$

$$k_{dis,XX} = -\frac{1}{\left(\Delta\langle T\rangle_{xx}/L_{ref,X}\right)}\frac{\rho_f C_{pf}}{V}\int\int\left(T_f - \langle T\rangle^f\right)\left(u - \langle u\rangle^f\right)\mathrm{d}V \tag{23}$$

$$k_{dis,YY} = -\frac{1}{\left(\Delta\langle T\rangle_{yy}/L_{ref,Y}\right)}\frac{\rho_f C_{pf}}{V}\int\int\left(T_f - \langle T\rangle^f\right)\left(v - \langle v\rangle^f\right)\mathrm{d}V \tag{24}$$

$\langle T\rangle^s$and $\langle T\rangle^f$are intrinsic volume averaged temperature for solid and fluid phases. As can be seen from Eqs. (23) and (24), $\Delta T$is the macroscopic fluid temperature difference in X direction for longitudinal and Y direction for transverse dispersion. The heat transfer coefficient is found based on the intrinsic temperature difference between $\langle T\rangle^s$and $\langle T\rangle^f$while for determination of thermal dispersion the local deviations of fluid temperature and the velocity from the volume averaged values are taken into account. Furthermore, it should be mentioned that Re number in this study is defined based on the cell size as:

$$\mathrm{Re} = \frac{\langle u\rangle d_c}{\nu} \tag{25}$$

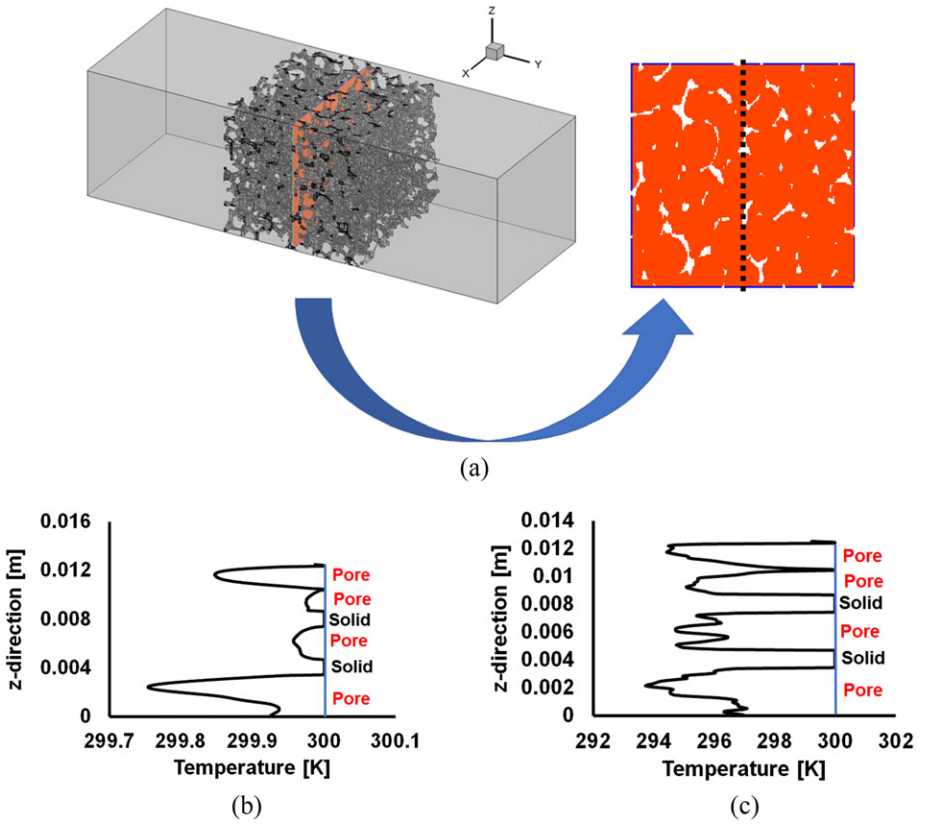

Figure 7. The temperature profiles on the line at the mid-point for 20 PPI metal foam; (*a*) the considered line to plot the temperature profile, (*b*) the temperature profile at the mid-plane [black dash line in (*a*)] when Re = 0.001, (*c*) the temperature profile at the mid-plane [black line in (*a*)] when Re = 600.

where the value of $d_c$for the studied metal foam is given in Table 1. Furthermore, the volumetric interfacial Nusselt number in this study is defined as

$$\mathrm{Nu}_v = \frac{h_v d_c^2}{k_f} \tag{26}$$

where h_v is the volumetric interfacial heat transfer coefficient.

4. Results

In this section, after validating of the numerical study, the obtained results for the interfacial convective heat transfer coefficient and longitudinal and transverse thermal dispersion will be discussed separately.

4.1. Grid independency and validation

Figure 5 shows the change in the resolution of digitalized metal foam (PPI =20) with the number of grids for the middle slice. By changing of the number of grids from 48^3 to 148^3, the generated structure details considerably changes. As it can be seen, not only the size but also the location of solid and voids also change. However, by changing of number of grids from 148^3 to 192^3 or even 250^3, the size and location of ligaments do not vary much, indicating independency of generated

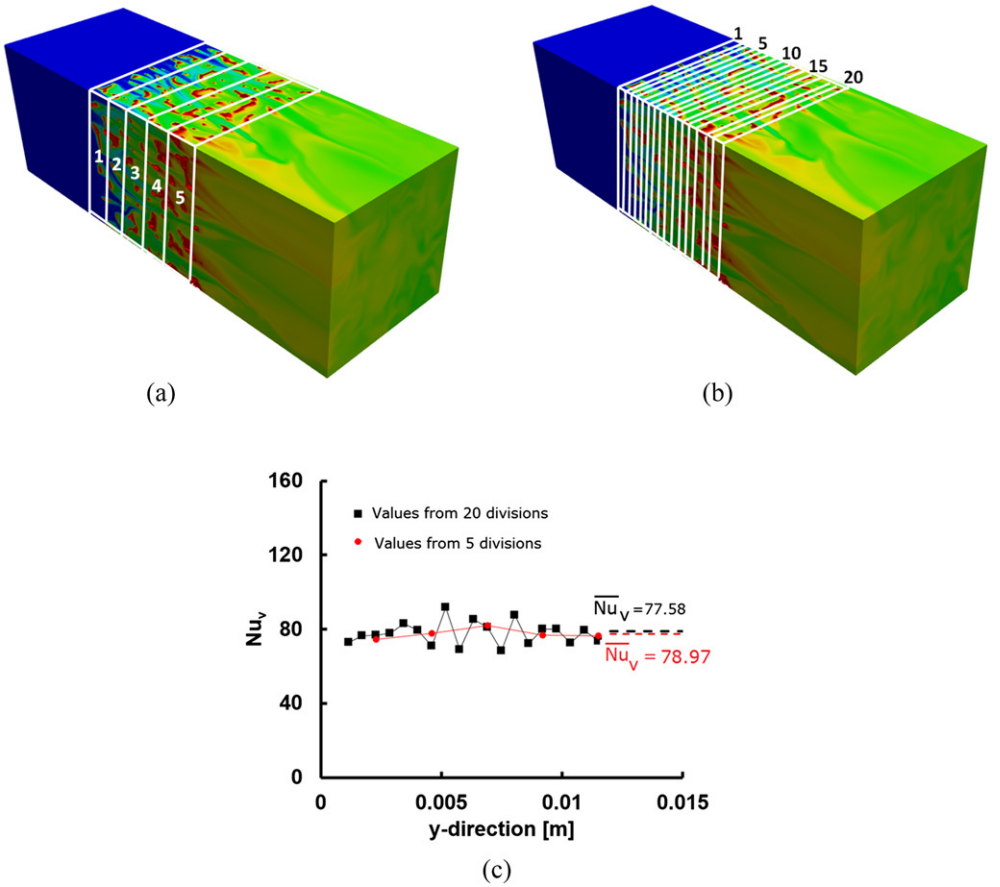

Figure 8. The change of volume averaged parameters with number of sub-volume for the sample with 20 PPI when Re = 600; (*a*) 5 sub-volumes domain, (*b*) 20 sub-volumes domain, (*c*) the change of interfacial Nusselt numbers with number of sub-volumes.

structure from the mesh. Furthermore, the interfacial convective heat transfer coefficient and longitudinal thermal dispersion are calculated for different grid numbers from $24 \times 24 \times 24$ to $250 \times 250 \times 250$ number when Re number is 600, and the changes are shown in Figure 6*a*, *b*, respectively. As it can be seen, a cell number around 7×10^6 is sufficient to have accurate results for determination of interfacial heat transfer and thermal dispersion coefficients.

Similar to the flow in channel and pipe due to temperature difference between solid and fluid, there should be a temperature gradient near the metal foam solid surface (particularly at the inlet region of the porous media) and by increase of the pore scale Re number, the temperature gradient near the surface region should become steeper. There should be a sufficient number of voxels in the pores to deduce this fact. Figure 7 shows the temperature profile in the middle line of a cross section existing in the middle of metal foam as shown in Figure 7*a*. Temperature profiles for Re = 0.001 is shown in Figure 7*b*. A smooth temperature gradient exists in the pores, and for this reason, the increase of temperature in the region close to the surface can be seen clearly. By increasing of Re number from 0.001 to 600, the gradient of velocity near the surface considerable increases and furthermore, fluctuations can be seen due to the collision of flow to the anterior ligament (Figure 7*c*). This figure provides a confidence on the employed number of voxels in the pores to catch the real behavior of the heat and flow in the pores.

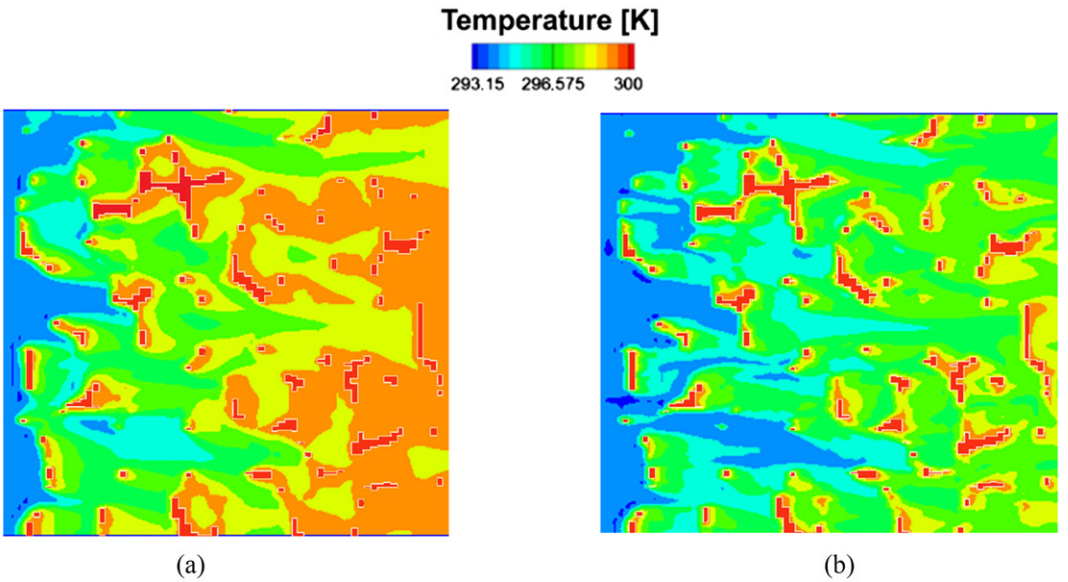

Figure 9. A sample of temperature distribution of metal foam for calculation of interfacial heat transfer coefficient and thermal dispersion for $z = L/2$, (*a*) Re =150, (*b*) Re = 600.

4.2. Interfacial heat transfer coefficient

Figure 8*a*, *b* shows temperature distribution in the computational domain with 20 PPI pore density aluminum foam when Re =600. The temperature at the inlet dummy region is cold and remains at inlet temperature without any change. The fluid enters into the foam region and its temperature increases due to the hot structure of solid phase in the region. After foam region, the fluid flows through the end of the channel and volume averaged temperature in this region does not change.

As it was mentioned before, the solid is maintained at the constant temperature which is greater than the fluid one. Hence a longitudinal temperature gradient in flow direction is generated. The division of aluminum foam is done in macroscopic heat flow direction, in other words in the direction in which macroscopic temperature gradient exists. Then, the interfacial heat transfer coefficient for each sub-volume is calculated by using Eq. (22). In this study, the aluminum foam domain is divided into 5 and 20 sub-volumes and Eq. (22) is applied to each sub-volume as can be seen from Figure 8*a*, *b*. The calculated interfacial heat transfer coefficient for each sub-domain of both sub-volumes is presented in Figure 8*c*. The average values for sub-volumes of domain divided by 5 and 20 are almost identical. An important result of Figure 8*c* is that the local interfacial Nusselt number between the solid and fluid changes around the same value. It does not have a trend such that starts with a high value and then becomes constant. This behavior of interfacial Nusselt number shows that a thermally fully developed condition exists, and the length of entrance region is negligible.

Figure 9 shows the temperature distribution at the center of the metal foam ($Z = 3L/2$) for Re = 150 and 600. The fully red spaces show solid which is hot. The temperature around hot solid is greater than its surrounding which is air. Furthermore, the effect of convection can be clearly observed from the shape of isotherms since by increasing of Re number, the convention effect along the flow direction become stronger. It should be noted that there must be a sufficient fluid temperature gradient between solid and fluid phases for calculation of Nu_v, otherwise numerical errors might be involved, and the obtained results might be questionable. In general, the study should be repeated for different solid and fluid phase temperatures to obtain a proper temperature difference.

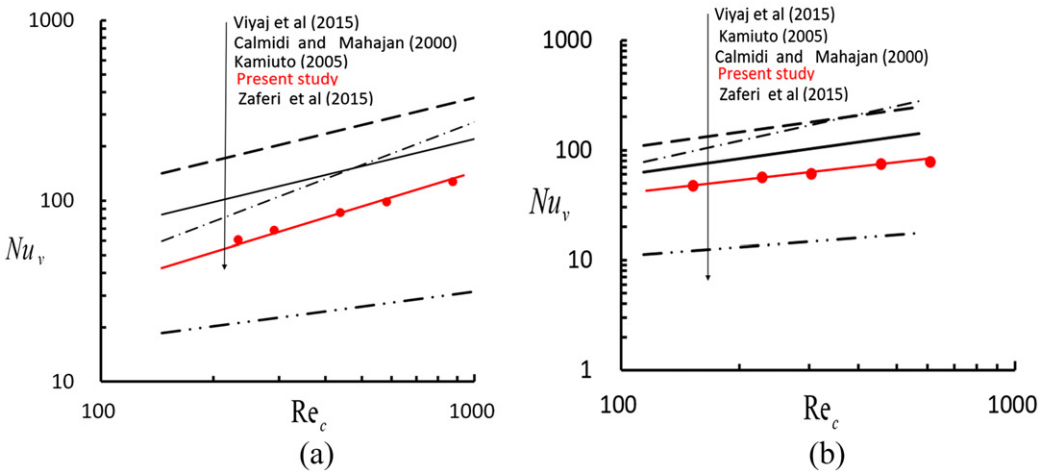

Figure 10. The comparison of volume interfacial Nusselt number of the present study with reported correlations, (*a*) 10 PPI, (*b*) 20 PPI.

The available correlations in the literature relating to the open cell metal foam are given in Table 2. As it can be seen, the considered characteristic length for the interfacial Nusselt number changes by researcher. Calmidi and Mahajan [13] selected strut diameter as characteristic length while Zafari et al. [11] chose the square root of permeability. Kamiuto and Yee [12] attempted to define a new characteristic parameter to combine different geometrical parameters of the cellular porous media. Vijay et al. [9] chose d_f/a_{sf}

(strut diameter/surface area) area as characteristic length for Nu_v for ceramic foams. These studies show that there is no consistency in the characteristic length of open cell foams because of the complexity of geometry. Finding an appropriate characteristic length is an issue which is out of the scope of present study. However, in order to compare the results of this study with available correlations in literature cell diameter (d_c) is selected and all suggested correlations are converted to have the same definition of Nu_v. The definition of cell diameter can be understood from Figure 2. It should be mentioned that some researchers have called this parameter as pore diameter as mentioned by Sajid Hossain and Shabani [21]. Figure 12 shows the comparison of the present results with the suggested correlations. As can be seen, there is a big difference between the suggested correlations which is normal. The cell diameter of different foams might be the same however the surface area, porosity, strut diameters, number of the strut in a cell and number of connections might be considerably different. These differences cause a considerable gap between the value of interfacial heat transfer coefficient of different correlations. Even if the strut diameter is selected as characteristic length, the same inconsistency will be observed due to the same reasons. Figure 10 shows that for both 10 and 20 PPI metal foam, the results of present study have relatively good agreement with the correlation suggested by Calmidi and Mahajan [13] and Kamiuto and Yee [12]. The obtained results are far from the correlation suggested by Vijay et al. [9] since they performed their study for ceramic foam. For metal foam with 10 and 20 PPI the maximum difference between the results of Calmidi and Mahajan [13], and present study is 75% and 46%, respectively.

4.3. Longitudinal thermal dispersion

The obtained results of longitudinal thermal dispersion by using Eq. (23) for 10 and 20 PPI aluminum foams are compared with the correlation of Zhang et al. [16] given in Table 2 and shown in Figure 11. To the best of our knowledge, their suggested equation is the only correlation

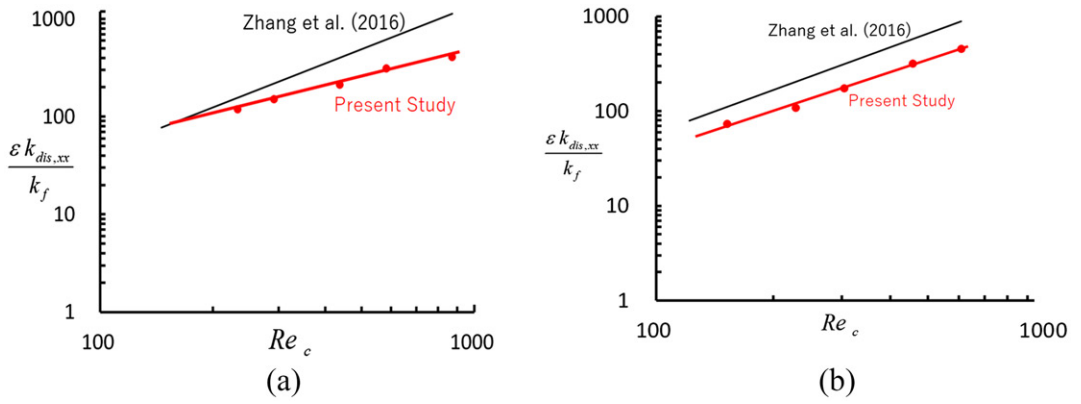

Figure 11. The comparison of longitudinal thermal dispersion of the present study with the reported correlations by Zhang et al. [16], (*a*) 10 PPI, (*b*) 20 PPI.

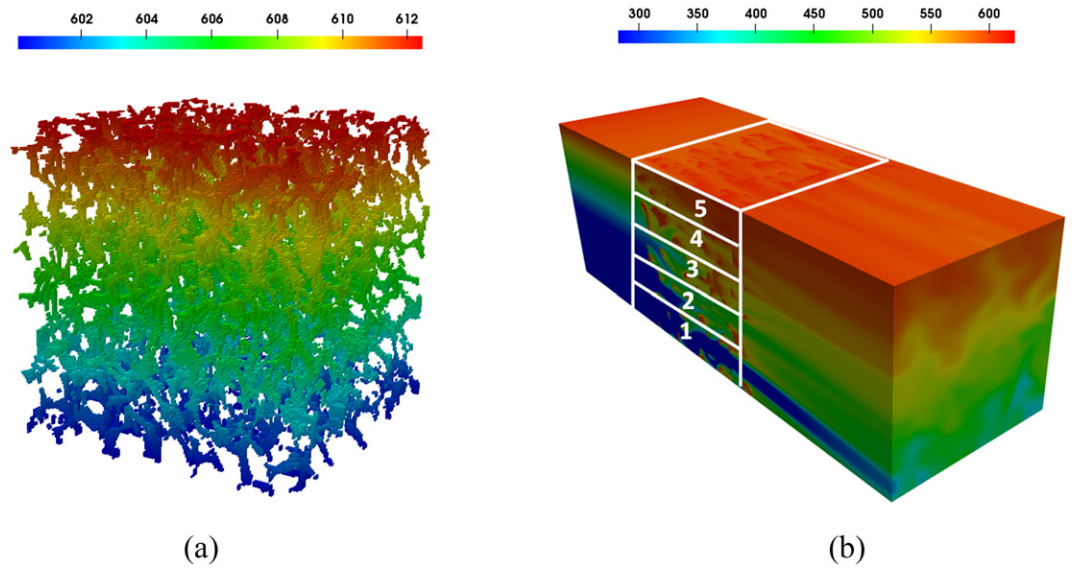

Figure 12. Temperature gradient in transverse direction for $k_{disp,YY}$ (*a*) linear transverse temperature gradient of the solid phase, (*b*) division of the domain in *X* direction.

relating to the longitudinal thermal dispersion of the metal foams in literature. Unfortunately, no experimental study could be found on the longitudinal thermal dispersion of the metal foams. The same velocity and temperature distribution used to obtain the interfacial heat transfer coefficient is employed for the determination of longitudinal thermal dispersion. The deviation of velocity and temperature from the volume averaged value is calculated and integrated over the entire domain. Then, it is divided by the macroscopic longitudinal temperature difference for each division (see Figure 8*a*). It should be mentioned that the integration is done for a subdomain in which a linear macroscopic temperature difference exists. The suggested correlation by Zhang et al. [16] mainly depends on the porosity and Re number, and the effects of other parameters (such as heat transfer area, ligament diameter, the connection of ligaments or pore to throat ratio size, etc.) have not been taken into account. Hence, some differences between the two results are expected. The agreement between the present results and the suggested correlation is

Table 2. The original and modified correlations for determination of interfacial heat transfer coefficient, longitudinal and transverse thermal dispersion of metal foam.

	Original equation	Modified volumetric interfacial Nusselt number	Remarks
Interfacial heat transfer coefficient			
Calmidi and Mahajan [13]	$\mathrm{Nu}_{d_f} = \frac{h d_f}{k_f} = C_T \mathrm{Re}_f^{0.5} \mathrm{Pr}^{0.37}$ $C_T = 0.52$	$\mathrm{Nu}_v = \frac{h_v d_c^2}{k_f} = C \mathrm{Re}_c^{0.5} \mathrm{Pr}^{0.37}$ $C = 0.52 a_{sf} \frac{d_c^{1.5}}{d_f^{0.5}}$	The study has been performed experimentally
Zafari et al. [11]	$\mathrm{Nu}_K = \frac{h\sqrt{K}}{k_f} = 0.016 + 0.16\varepsilon^{-3} \mathrm{Re}_K^{0.28}$	$Nu_v = \frac{h_v d_c^2}{k_f} = C_1 + C_2 \mathrm{Re}_c^{0.28}$ $C_1 = 0.016 a_{sf} \frac{d_c^2}{\sqrt{K}}$ $C_2 = a_{sf} \frac{0.16}{\varepsilon^3} \frac{d_c^{1.72}}{K^{0.38}}$	The values of permeability of the metal foams of this study are reported by Celik et al. [20]
Kamiuto and Yee [12]	$\mathrm{Nu}_s = \frac{h_v D_s^2}{k_f} = B(\mathrm{Re}_s \mathrm{Pr})^{0.791}$ $B = 0.124,\ D_s^* = 2\omega/\sqrt{\pi}\ ,\ D_s = D_c D_s^*$ $w = 0.5 + \cos((1/3)\cos^{-1}(2\varepsilon - 1) + (4\pi/3))$	$\mathrm{Nu}_v = \frac{h_v d_c^2}{k_f} = C(\mathrm{Re}_c \mathrm{Pr})^{0.791}$ $C = B(\frac{D_s}{d_c})^{1.209}$	The study has been performed by utilizing different available results in literature
Vijay et al. [9]	$\mathrm{Nu}_v = \frac{h_v d_{str}}{a_s k_{fe}} = C_t \mathrm{Re}_{d_{str}}^{0.5} \mathrm{Pr}_{fe}^{0.37}$ $C_t = 0.94$	$\mathrm{Nu}_v = \frac{h_v d_c^2}{k_f} = C \mathrm{Re}_c^{0.5} \mathrm{Pr}_f^{0.37}$ $C = C_t a_{sf} \frac{d_c^{1.5}}{d_{str}^{0.5}} (\frac{k_{fe}}{k_f})^{0.63}$	The study has been performed experimentally
Longitudinal thermal dispersion			
Zhang et al. [16]	$\frac{\varepsilon k_{dis_{yy}}}{k_f} = 0.043 \frac{(\frac{\rho c(u) d_m}{k})^{3/2} \mathrm{Pr}^{0.13}}{(1-\varepsilon)^{0.25} (\frac{1-e^{-(1-\varepsilon)/0.04}}{\varepsilon})^{1/2}}$	$\frac{\varepsilon k_{dis_{xx}}}{k_f} = C \mathrm{Re}_{d_m}^{1.5} \mathrm{Pr}^{1.63}$ $C = \frac{0.043}{(1-\varepsilon)^{0.25} (\frac{1-e^{-(1-\varepsilon)/0.04}}{\varepsilon})^{1/2}}$	The correlation suggested by Calmidi and Mahajan [13] has been used to find longitudinal thermal dispersion
Transverse thermal dispersion			
Calmidi and Mahajan [13]	$\frac{k_d}{k_e} = C_D (\mathrm{Re}_K \mathrm{Pr}_e) \frac{u}{u_o}$ $C_D = .0.06$	$\frac{\varepsilon k_d}{k_f} = C(\mathrm{Re}_{d_m} \mathrm{Pr}_f)$ $C = C_D \frac{\varepsilon\sqrt{K}}{d_m} \frac{k_f}{k_e}$	The study has been performed experimentally. The values of permeability of the studied metal foams are reported in Celik et al. [20]
Zhang et al. [16]	$\frac{\varepsilon k_{dis_{yy}}}{k_f} = 0.000191 \frac{(\frac{\rho c(u) d_m}{k})^{3/2} \mathrm{Pr}^{0.13}}{(1-\varepsilon)^{0.25} (\frac{1-e^{-(1-\varepsilon)/0.04}}{\varepsilon})^{1/2}}$	$\frac{\varepsilon k_{dis_{yy}}}{k_f} = C \mathrm{Re}_{d_m}^{1.5} \mathrm{Pr}^{1.63}$ $C = \frac{0.000191}{(1-\varepsilon)^{0.25} (\frac{1-e^{-(1-\varepsilon)/0.04}}{\varepsilon})^{1/2}}$	The correlation suggested by Calmidi and Mahajan [13] has been used to find longitudinal thermal dispersion.

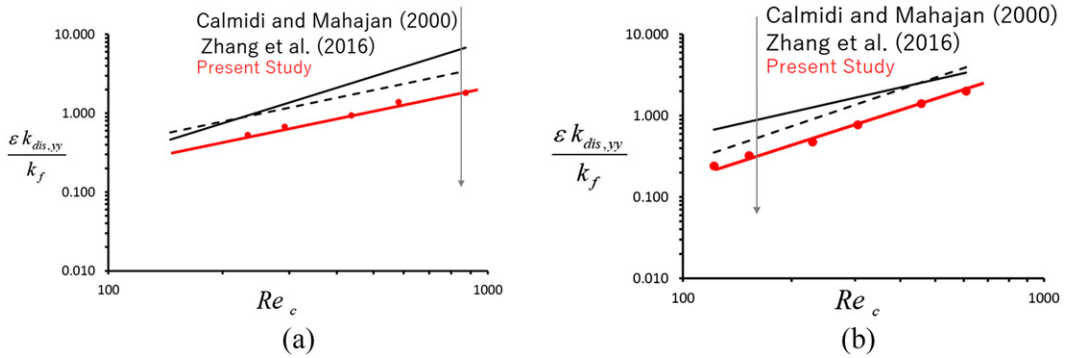

Figure 13. The comparison of obtained transverse thermal dispersion with two available correlations in literature (*a*) 10 PPI, (*b*) 20 PPI.

maximum 48%. The trend of the obtained results with the correlation is better for 20 PPI since it contains 125 cells while the sample of 10 PPI has only 27 cells.

4.4. Transverse thermal dispersion

Similar to the longitudinal thermal dispersion, the transverse thermal dispersion can be by found by Eq. (24). A transverse macroscopic temperature gradient is generated in transverse direction as can be seen from Figure 12*a* since Eq. (24) requires macroscopic linear temperature. Then, the micropore governing equations are solved, and temperature and velocity distributions are found (Figure 12*b*). Eq. (24) can be applied to each division (for metal foam region) of Figure 12*b* and of the transverse thermal dispersion is calculated. Although this method has been widely used by many researchers for the periodic structure (e.g., Nakayama et al. [14], Ozgumus et al. [8]), but our calculation showed that the obtained results by this method might not be correct for the stochastic porous media. The reason is the small values of v velocity (transverse velocity) and consequently small values of deviations. For instance, the value of $\langle v \rangle$ for the metal foam with 20 PPI is found as $1.2\mathrm{E}-9$, and total deviation $(\int\int(T_f - \langle T \rangle^f)(v - \langle v \rangle^f)dV)$ is $6\mathrm{E}-8$. This is an expected result since it is well known that transverse thermal dispersion is very smaller than longitudinal one. However, our observation showed that numerical errors considerably affect the computation results during calculation of transverse thermal dispersion, particularly for low values of Re number. Hence, the obtained results are not trustable. The assumption employed by Zhang et al. [16] can be a solution for this difficulty and helps to determine transverse thermal dispersion. They suggested that $k_{yy} = 15^2 k_{xx}$ and based on this assumption, the value of the transverse thermal dispersion can be found easily. Based on this assumption, the obtained results are compared with the correlation of Calmidi and Mahajan [13] and Zhang et al. [16]. These correlations are given in Table 2. These correlations are rewritten regarding the cell diameter Re number. A good agreement between the obtained results and suggested correlations of two studies can be seen from Figure 13.

5. Conclusion

The interfacial convective heat transfer coefficient, longitudinal and transverse thermal dispersion for 10 and 20 PPI aluminum metal foams are studied numerically. Metal foams are scanned using X-ray microtomography technique and 3D digital structure is achieved. Then, the pore scale conservation equations are solved for the obtained digital structure and the coefficients of thermal

dispersion and interfacial heat transfer for each metal foam are calculated by using volume average technique. The important conclusions of the study can be stated as:

- Various metal foam structures exist in market (cell size, ligament size and shape, porosity, connection nodes number, etc. are different). It is difficult to suggest a single correlation to cover all available structures in market. Hence, considerable differences between the results of suggested correlations are expected.
- For the interfacial heat transfer coefficient, a big difference between the suggested correlations in literature was observed. However, the obtained results of present study for the interfacial heat transfer coefficient is relatively close to the correlation of Calmidi and Mahajan [13] and Kamiuto and Yee [12]. Maximum difference from the correlation of Calmidi and Mahajan [13] is 75% for 10 PPI and 46% for 20 PPI aluminum foam.
- For longitudinal thermal dispersion of metal foam, only one correlation could be found in literature [16]. A good agreement between the result of this study and their correlation was observed. Maximum difference between this study with the suggested correlation is below the 48% for 10 and 20 PPI.
- Although temperature gradient in transvers direction is generated to calculate transverse dispersion, due to the extremely low values of transverse velocity and including of numerical errors, the trustable results could not be achieved. However, a proportional relationship existing between longitudinal and transverse thermal dispersions is used and the acceptable results for transvers thermal dispersion could be found.
- In general, the results of metal foam with 20 PPI is closer to the suggested correlations compared to 10 PPI. The reason might be the large number of cells of the sample with 20 PPI (125 cells for 20 PPI while 27 cells for 10 PPI).

Experimental determination of thermal transport parameters of stochastic porous media (particularly thermal dispersion conductivity) is a difficult task. Microthermography technique provides generation of digital structure in computer environment to calculate those properties. However further studies on the computational model and method (such as effect of number of cells, control volume thickness, remedy for extremely low values of velocity, effect of dummy regions, etc.) should be done to achieve more accurate results.

Acknowledgments

Hasan Celik would like to thank to the generous support of Scientific and Technological Research Council of Turkey (TUBITAK) under 2214/A fellowship. Furthermore, the supercomputer system of Academic Center for Computing and Media Studies of Kyoto University in Japan and TUBITAK ULAKBIM, High Performance and Grid Computing Center (TRUBA resources) in Turkey are used. The authors would like to express their gratitude to these organizations.

References

[1] P. Li, X. Fan, and Z. Chen, "Numerical study on the heat transfer of micro elliptic pin fins in a rectangular minichannel," Numer. Heat Transf. A, vol. 70, no. 11, pp. 1242–1252, 2016.

[2] Y. Yang, K. Tsai, H. Tang, and S. Chung, "Numerical simulations and optimization of porous pin fins in a rectangular channel," Numer. Heat Transf. A, vol. 70, no. 7, pp. 791–808, 2016.

[3] H. Celik, M. Mobedi, O. Manca, and U. Ozkol, "A pore scale analysis for determination of interfacial convective heat transfer coefficient from thin periodic porous media under mixed convection," Int. J. Numer. Methods Heat Fluid Flow, vol. 27, pp. 2775–2798, 2017.

[4] E. Ucar, M. Mobedi, G. Altintas, and E. Glatt, "Effect of voxel size in flow direction on permeability and Forchheimer coefficients determined by using micro-tomography images of a porous medium," Prog. Comput. Fluid Dyn., vol. 15, no. 5, pp. 327–333, 2015.

[5] K. B. Karthik, Y. M. Jayathi, and V. G. Suresh, "Microtomography-based simulation of transport through open-cell metal foams," Numer. Heat Transf. A, vol. 58, no. 7, pp. 527–544, 2010.
[6] F. Kuwahara, A. Nakayama, and H. Koyama, "A numerical study of thermal dispersion in porous media," ASME J. Heat Transf., vol. 118, pp. 756–761, 1996.
[7] M. B. Saito and M. J. de Lemos, "A correlation for interfacial heat transfer coefficient for turbulent flow over an array of square rods," ASME J. Heat Transf., vol. 32, pp. 666–676, 2005.
[8] T. Ozgumus and M. Mobedi, "Effect of pore to throat size ratio on interfacial heat transfer coefficient of porous media," ASME J. Heat Transf., vol. 137, p. 012602, 2015.
[9] D. Vijay, P. Goetze, R. Wulf, and U. Gross, "Forced convection through open cell foams based on homogenization approach: steady state analysis," Int. J. Therm. Sci., vol. 98, pp. 381–394, 2015.
[10] A. Zukauskas and J. Ziugzda, Heat Transfer of a Cylinder in Crossflow. Berlin: Springer, 1985.
[11] M. Zafari, M. Panjepour, M. D. Emami, and M. Meratian, "Microtomography-based numerical simulation of fluid flow and heat transfer in open cell metal foams," Appl. Therm. Eng., vol. 80, pp. 347–354, 2015.
[12] K. Kamiuto, and S. S. Yee, "Heat transfer correlations for open-Cellular Porous materials," Int. Commun. Heat Mass Transf., vol. 32, no. 7, pp. 947–953, 2005.
[13] V. Calmidi and R. Mahajan, "Forced convection in high porosity metal foams," ASME J. Heat Transf., vol. 122, no. 3, pp. 557–565, 2000.
[14] F. Kuwahara and A. Nakayama, "Numerical determination of thermal dispersion coefficients using a periodic porous structure," ASME J. Heat Transf., vol. 121, no. 1, pp. 160–163, 1999.
[15] T. Ozgumus and M. Mobedi, "Effect of pore to throat size ratio on thermal dispersion in porous media," Int. J. Therm. Sci., vol. 104, pp. 135–145, 2016.
[16] W. Zhang, W. Li, and A. Nakayama, "An analytical consideration of steady-state forced convection within a nanofluid-saturated metal foam," J. Fluid Mech., vol. 769, pp. 590–620, 2015.
[17] K. Vafai and C. L. Tien, "Boundary and inertia effects on flow and heat transfer in porous media," Int. J. Heat Mass Transf., vol. 24, no. 2, pp. 195–203, 1981.
[18] A. Nakayama, PC-Aided Numerical Heat Transfer and Convective Flow. Boca Raton, FL: CRC Press, 1995.
[19] C. Yang, K. Ando, and A. Nakayama, "A local thermal non-Equilibrium Analysis of fully developed forced convective flow in a tube filled with a porous medium," Transp. Porous Media, vol. 89, no. 2, pp. 237–249, 2011.
[20] H. Celik, "An experimental and numerical study on interfacial convective heat transfer coefficient and thermal dispersion conductivity of a periodic porous medium under mixed convection heat transfer," PhD thesis, Izmir Institute of Technology, Turkey, 2017.
[21] M. Sajid Hossain and B. Shabani, "Metal foams application to enhance cooling of open cathode polymer electrolyte membrane fuel cells," J. Power Sources, vol. 295, pp. 275–291, 2015.